Full band assessment of Phonon-limited mobility in graphene nanoribbons.

A. Betti, G. Fiori and G. Iannaccone
Dipartimento di Ingegneria dell'Informazione
Università di Pisa, Via Caruso I-56122 Pisa, Italy
Tel. +39 050 2217639; Fax. +39 050 2217522, email: alessandro.betti@iet.unipi.it

***Abstract*— We present a full band investigation of electron-phonon interaction in Graphene NanoRibbons (GNRs) by exploiting a tight-binding description within the deformation potential approximation. We show that a full band approach is required to obtain accurate results: mobility as high as 800 cm^2/Vs at room temperature can be achieved for 1 nm-wide ribbons, more than one order of magnitude higher than that obtainable in silicon nanowires, but still not enough to ensure ballistic transport in GNR-based devices.**

I. Introduction

Graphene NanoRibbons (GNRs) continue to attract much attention, since lateral confinement represents one of the few available options to induce a reasonable gap in graphene, even if lithographic precision at the level of single atom is required. To assess their perspective for use in nanoelectronics, it is also essential to evaluate their intrinsic mobility, especially as new promising methods able to prepare defect-free samples are developed [1]. This issue is still open, and represents the main motivation for our work.

Here, we provide a detailed investigation of the intrinsic electron-phonon interaction by means of a full band (FB) analysis, based on a tight-binding (TB) description of the electronic structure and phonon dispersion curves [2]. Building upon significant advancements with respect to previous models appeared in the literature [3], [4], [5], here we have included the effect of both the in-plane acoustic (AC) and optical (OP) modes L and T, intersubband scattering, the transverse momentum conservation uncertainty, and the two-component nature (spinor) of the nanoribbon wavefunction.

II. Methodology

The energy dispersion of armchair GNRs has been obtained through a tight-binding p_z-Hamiltonian accounting for energy relaxation at the edges [2]. Graphene phonon spectrum has been derived by means of the force-constant dynamic-matrix approach, including contributions up to the fourth nearest neighbor interactions and exploiting parameters extracted from first-principles calculations [6]. For a GNR with l dimer lines in the transverse direction y, each of the 6 phonon branches of graphene, labelled by the quantum number j ($j = 1-3$ for AC and $j = 4-6$ for OP branches, respectively) is splitted into l sub-branches in the nanoribbons, each corresponding to a different transverse wavevector $q_{y\beta}$ ($q_{y\beta} = (2\pi\beta)/[(l+1)a]$ for $\beta = 0, ..., l/2-1$ and $q_{y\beta} = [2\pi(\beta+2)]/[(l+1)a]$ for $\beta = l/2, ..., l-1$).

Scattering rates have been computed by means of the Fermi Golden Rule, within the deformation potential approximation (DPA) and exploiting a collisional broadening approach for small AC phonon energies. The momentum relaxation rate for an electron in the initial state $\mathbf{k} = (k_x, k_{y\eta})$, with $\eta = 1, ..., l$, is obtained by considering all transitions involving phonons of the $6l$ sub-branches (j, β) for all final electron states $\mathbf{k'} = (k_x, k_{y\eta'})$ [7]:

$$\frac{1}{\tau(\mathbf{k})} = \sum_{\eta'=1}^{l} \sum_{j=1}^{6} \sum_{\beta} \frac{n_{\mathbf{q}}^{\mp}\, \hbar D_{AC}^2}{4\rho W E_{ph}^{j\beta}} \left(1+\cos\theta_{\mathbf{kk'}}\right)\left(1-\cos\alpha\right)$$
$$G_{\eta,\eta',\beta} \int_{-k_F}^{+k_F} dq_x \left(q\,\delta_{j,AC} + \frac{2\pi}{a}\delta_{j,OP}\right)^2 \delta_D\left[E\left(k_x \pm q_x, k_{y\eta'}\right)\right.$$
$$\left. -E\left(k_x, k_{y\eta}\right) \mp E_{ph}^{j\beta}\left(q_x, q_{y\beta}\right)\right] \frac{1-f\left[E\left(k_x \pm q_x, k_{y\eta'}\right)\right]}{1-f\left[E\left(k_x, k_{y\eta}\right)\right]}, \quad (1)$$

where $k_{y\eta} = (2\pi\eta)/[(l+1)a]$ is the transverse electron momentum, D_{AC} and $D_{OP} = (2\pi)/a\, D_{AC}$ are the AC and OP deformation potentials, respectively, whereas $n_{\mathbf{q}}^{+} = n_{\mathbf{q}}^{-} + 1$, $n_{\mathbf{q}}^{-}$ is the Bose-Einstein occupation factor, $\rho = 7.6 \times 10^{-8}$ g/cm^{-2} is the mass density of graphene, W is the GNR width, $k_F = \pi/(\sqrt{3}\,a)$, $a = \sqrt{3}\,a_{CC}$ ($a_{CC} = 0.144$ nm) and $\theta_{\mathbf{kk'}}$ is due to the spinor nature of the GNR wavefunction [7]. $\delta_{j,AC}$ ($\delta_{j,OP}$) is the Kronecker delta: $\delta_{j,AC} = 1$ ($\delta_{j,OP} = 1$) if $j = 1, ..., 3$ ($j = 4, ..., 6$), 0 otherwise. For narrow ribbons, backscattering limits the angle α between $\mathbf{k}$ and $\mathbf{k'}$ to $\alpha = \pi$.

In Eq. (1), $G_{\eta,\eta',\beta}$ is the form factor due to the transverse momentum conservation uncertainty:

$$G_{\eta,\eta',\beta} = \frac{2\left[4\pi^3\beta\,\eta\,\eta'\right]^2\left[1-(-1)^{\eta+\eta'+\beta}\right]}{\left[(\pi\beta)^4 - 2\pi^4\beta^2\left(\eta^2+\eta'^2\right) + \pi^4\left(\eta^2-\eta'^2\right)^2\right]^2}, \quad (2)$$

peculiar of 1D systems [8]. The low-field mobility has been finally calculated adopting the Kubo-Greenwood formalism [9]:

$$\mu = \frac{e}{\pi^3 k_B T \hbar^2 n_{2D} W} \sum_{\eta=1}^{l} \int_{-k_F}^{+k_F} dk_x \frac{\tau(\mathbf{k})}{\left[D_\eta(\mathbf{k})\right]^2} f\left(E_{\mathbf{k}}\right)\left[1-f\left(E_{\mathbf{k}}\right)\right], \quad (3)$$

where $1/\tau(\mathbf{k})$ is the inverse lifetime of an electron with initial momentum $\mathbf{k}$ and energy $E_{\mathbf{k}}$ (Eq. (1)), whereas n_{2D} is the quasi-1D electron concentration due to the finite width of the nanoribbon, T is the temperature and $D_\eta(k_x, k_{y\eta}) = 1/\pi\,[dk_x/dE_\eta(k_x, k_{y\eta})]$ is the 1D density of states (DOS) for the η-th electron subband.

III. Results and Discussions

The GNR phonon sub-branches (both AC and OP) are sketched in Fig. 1 for different widths W, ranging from 1 to 10 nm, obtained from the zone folding of the six branches of graphene phonon dispersion: longitudinal (L), transversal (T) and flexural modes (Z).

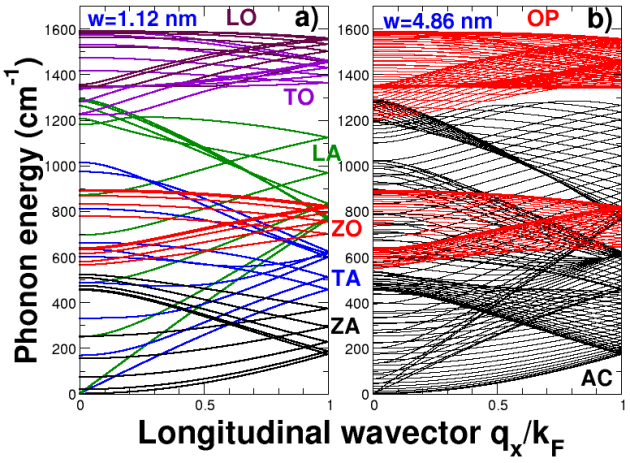

Fig. 1. Phonon dispersion curves for two different GNR widths: $W = 1.12$ nm (a) and $W = 4.86$ nm (b). In (a) different colors correspond to different types of in-plane and out-of-plane vibrations. In (b) black (red) curves refer to AC (OP) sub-branches.

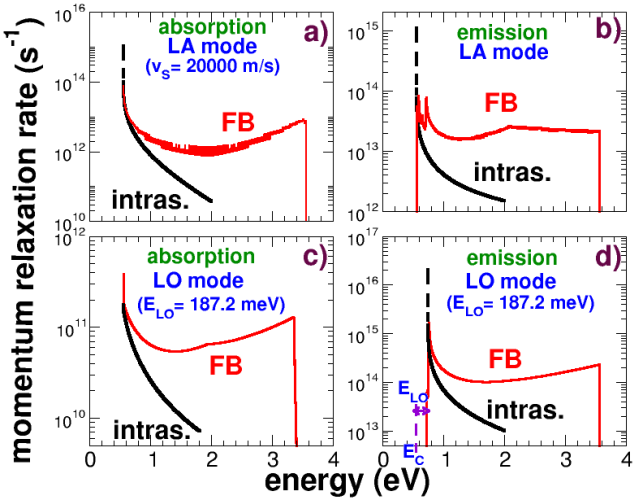

Fig. 2. Intrasubband scattering rates obtained by means of the FB approach (Eq. (1)) for the lowest conduction subband for $W = 1.12$ nm. Intrasubband AC intravalley and OP scattering rates obtained as in Ref. [3] are also shown (black dashed lines).

Figs. 2a-d show a comparison between the scattering rates obtained by means of our FB approach and of the analytical approach proposed in Ref. [3] for $W = 1.12$ nm. Only the LA and LO modes are taken into account, and for a fair comparison the very same phonon parameters as in Ref [3] are assumed. As can be seen, results in [3] largely underestimate the scattering rate: this clearly calls for the adoption of the FB approach.

The general assumption made in literature for AC modes is that only LA phonons limit mobility [3] [4]. However, very recently DFT calculations [12] and models based on group theory [13] have demonstrated that TA mode plays an important role. As a consequence, we have directed our efforts towards the determination of an effective deformation potential D_{AC} within the DPA approximation taking into account LA as well TA modes. Such choice has been driven by the fact that a large range of D_{AC} values are available in the literature for graphene, ranging from 4.75 eV [14] to 29 eV [15]. In the extreme uncertainty concerned with the actual intrinsic graphene mobility in experiments, density functional theory (DFT) represents the method of choice to quantitatively evaluate the right D_{AC} parameter. To this purpose, in the following, we use $D_{AC} = 4.5$ eV [12], computed by means of DFT simulations and consistent with those calculated within the Su-Schrieffer-Heeger (SSH) model ($D_{AC} \approx 7.4$ eV) [16] and by fitting to experimental data ($D_{AC} \approx 4.75$ eV) [14]. In this work, we neglect flexural modes which are negligible for temperature higher than 130 K, according to [10] and [11].

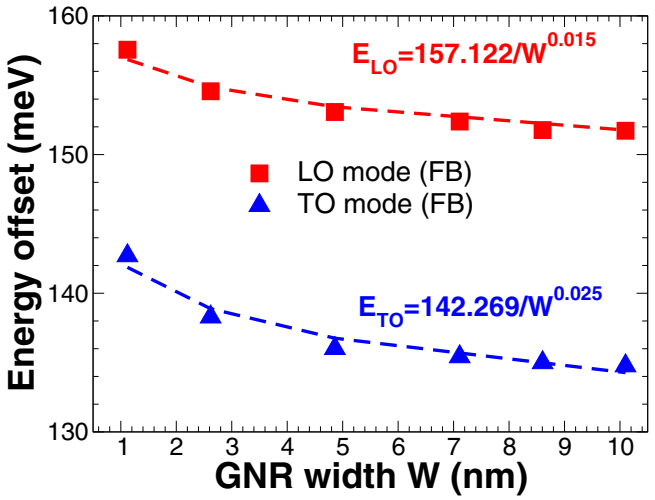

Fig. 3. Optical energy offset as a function of W for the TO (blu triangles) and LO (red squares) modes. Dashed lines correspond to the fitting.

In Fig. 3 the computed OP energy offset is shown as a function of W for the LO and TO modes, where $E_{LO}, E_{TO} \propto 1/W^{\alpha}$, with $\alpha \approx 0.02$. Our calculated E_{LO} agrees with those generally used in literature [3], [4] (152-160 meV).

The general assumption made when studying mobility in GNRs is that forward scattering ($\alpha = 0$) is arbitrarily neglected. Here we want to verify such assumption. In particular, phonon-limited mobility for $W = 4.86$ nm and 10.10 nm as a function of the carrier density n_{2D} by including only backscattering and backward+forward scattering is shown in Figs. 4a-b. As can be seen, forward scattering can be reasonably neglected for width up to $W = 10$ nm.

The total mobility and the AC and OP phonon-limited mobility (μ, μ_{AC} and μ_{OP}, respectively) are shown in Fig. 5 as a function of n_{2D}. For the narrower GNRs, μ is close to 800 cm^2/Vs (Fig. 5a) and is mainly limited by AC phonons (Fig. 5b). For narrow ribbons the larger n_{2D}, the larger μ, because of the larger intrasubband scattering time τ. Instead, for wider GNRs, intersubband scattering is activated in the inversion regime, due to the increased density of states available for scattering, reducing μ. For $n_{2D} > 10^{12}$ cm^{-2}, the degeneracy factor $[1-f(E_{\mathbf{k}'})]/[1-f(E_{\mathbf{k}})]$, often neglected in literature, has to be considered. μ_{AC} and the mobility limited by TA (μ_{TA}) and LA (μ_{LA}) phonons are shown in Fig. 6, as a function of n_{2D} for different W: $\mu_{TA} < \mu_{LA}$, for any n_{2D}.

In Fig. 7a-b, μ is plotted as a function of W for different n_{2D} and T, respectively. As also observed in small-diameter CNTs [16], the dependence on W and T in narrow

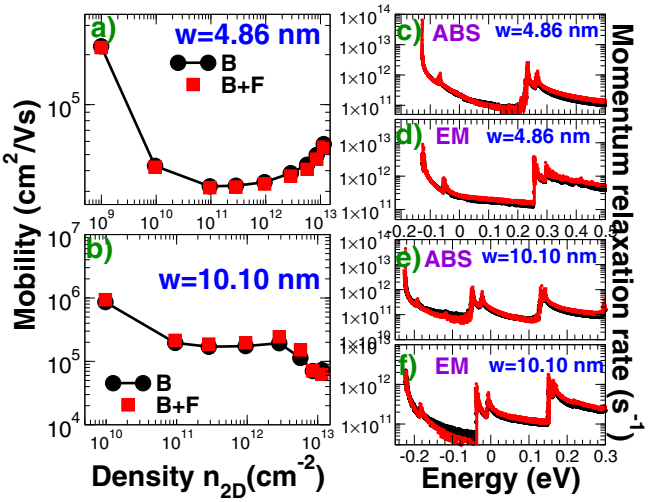

Fig. 4. Mobility as a function of n_{2D} computed including only the backward (B) and both the forward and backward (F+B) scattering for $W = 4.86$ nm (a) and 10.10 nm (b). (c)-(f): momentum relaxation rates corresponding to absorption (ABS) and emission (EM) of AC phonons calculated for B and F+B for the first conduction subband of 4.86 nm and 10.10 nm-wide GNRs. $n_{2D} = 9 \times 10^{12}$ cm^{-2}.

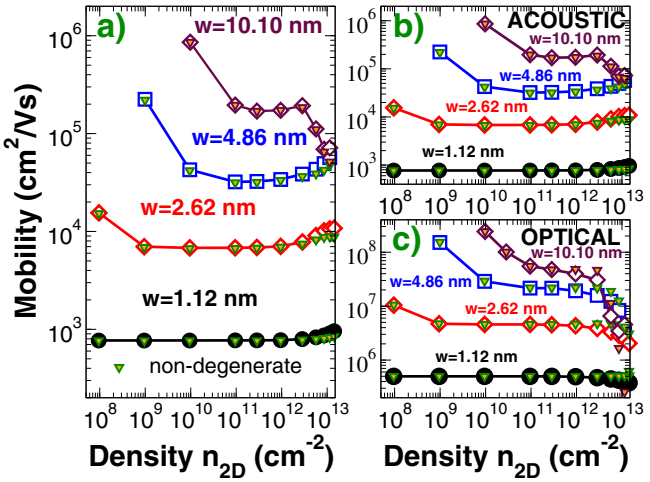

Fig. 5. a) Total mobility, (b) acoustic and (c) optical phonon-limited mobility as a function of n_{2D} for different W. The mobility computed for non-degenerate semiconductor is also shown (triangles).

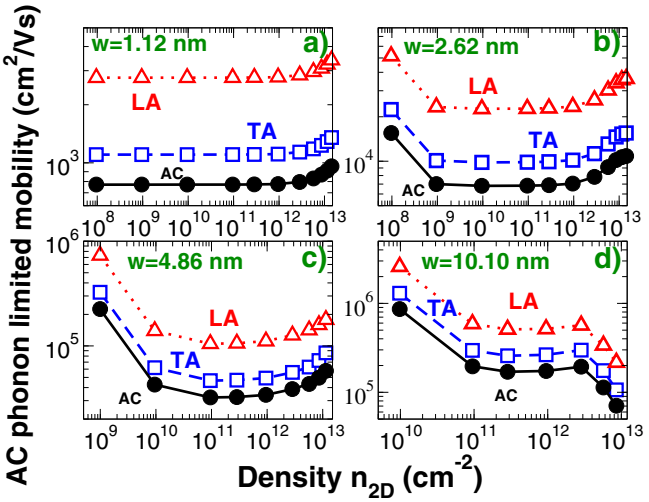

Fig. 6. FB mobility limited by TA and LA phonons and total AC phonon-limited mobility μ_{AC} as a function of n_{2D} for different W.

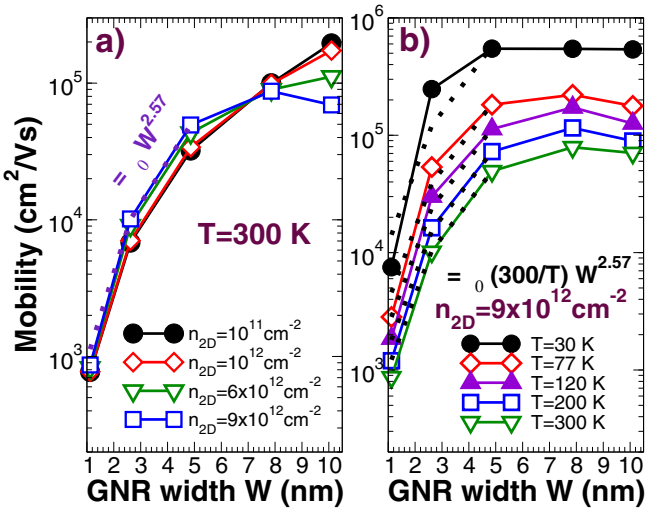

Fig. 7. (a): Mobility as a function of W for different n_{2D}. T=300 K. (b): mobility as a function of W for different T, $n_{2D} = 9 \times 10^{12}$ cm^{-2}. In both plots dotted lines represent the fitting with $\mu(W,T) = \mu_0\,(W/1\,\mathrm{nm})^{\alpha}$.

GNRs can be described by the empirical relation $\mu(W,T) = \mu_0\,300\,\mathrm{K}/T\,(W/1\,\mathrm{nm})^{\alpha}$, where $\mu_0 \approx 500$ cm^2/Vs and $\alpha = 2.57$. For narrow GNRs or in the subthreshold regime, $\mu \propto G^{-1} \propto W^2$. For larger W and in the inversion regime, μ saturates (Fig. 7a), since the number of subbands contributing to μ rapidly increases, due to the Pauli blocking factor $f(1-f)$, and the DOS tends to the 2D value (DOS $\propto W$). For a fixed W the smaller the T, the larger the μ, since $\mu \propto 1/n_{\mathbf{q}}^{-}$ (Fig. 7b).

According to AC in-plane phonon scattering, μ shows an inverse dependence on T since $n_{\mathbf{q}}^{-} \approx kT/\hbar\omega$ for $kT \gg \hbar\omega$ (Fig. 8a). Fig. 8b shows the mean coherence length $\langle L_{\mathbf{k}} \rangle$, defined as

$$\langle L_{\mathbf{k}} \rangle = \frac{\int_{-k_F}^{k_F} dk_x\, v(\mathbf{k})\, \tau(\mathbf{k})\, f(E_{\mathbf{k}})\,(1 - f(E_{\mathbf{k}}))}{\int_{-k_F}^{k_F} dk_x\, f(E_{\mathbf{k}})\,(1 - f(E_{\mathbf{k}}))}, \qquad (4)$$

where $v(\mathbf{k}) = 1/\hbar\,(\partial E_{\mathbf{k}}/\partial \mathbf{k})$ is the band velocity. $\langle L_{\mathbf{k}} \rangle$ increases by up to one order of magnitude within the considered interval and can be of the order of tens of nanometers (Fig. 8b) for narrower GNRs, relaxing the ballistic assumption generally made for ultrashort devices.

Figs. 9a-b show $L_{\mathbf{k}}$ as a function of $E_{\mathbf{k}}$ and $\langle L_{\mathbf{k}} \rangle$ as a function of W in the strong inversion regime ($n_{2D} = 9 \times 10^{12}$ cm^{-2}) for the lowest two conduction subbands, whereas Fig. 9c shows instead $\langle L_{\mathbf{k}} \rangle$ as a function of n_{2D} for the lowest subband. $L_{\mathbf{k}}$ exhibits a strong energy dependence, with a wide maximum at low energies (Fig. 9a). $\langle L_{\mathbf{k}} \rangle$ increases about two orders of magnitude with W, saturating to few thousands of nanometers for the wider GNRs (Fig. 9b). $\langle L_{\mathbf{k}} \rangle$ tends also to increase with n_{2D}, saturating for the wider ribbons in the strong inversion regime (Fig. 9c).

Finally, we compare the computed mobility for $n_{2D} = 10^{12}$ cm^{-2} with experimental results available in literature for GNR, CNT and SNW (Fig. 10). First, AC phonons are not the most limiting factor in narrow GNRs. Second, intrinsic mobility in GNR is lower than in CNT, but higher than in silicon-based technology.

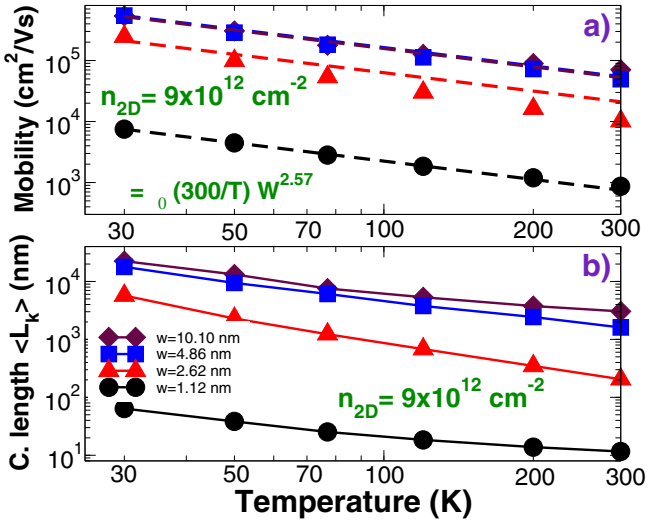

Fig. 8. (a) Mobility and (b) mean coherence length $\langle L_{\mathbf{k}} \rangle$ as a function of T for different W. In (a) dashed lines correspond to the linear fit. In (a) and (b) $n_{2D} = 9 \times 10^{12}$ cm^{-2}.

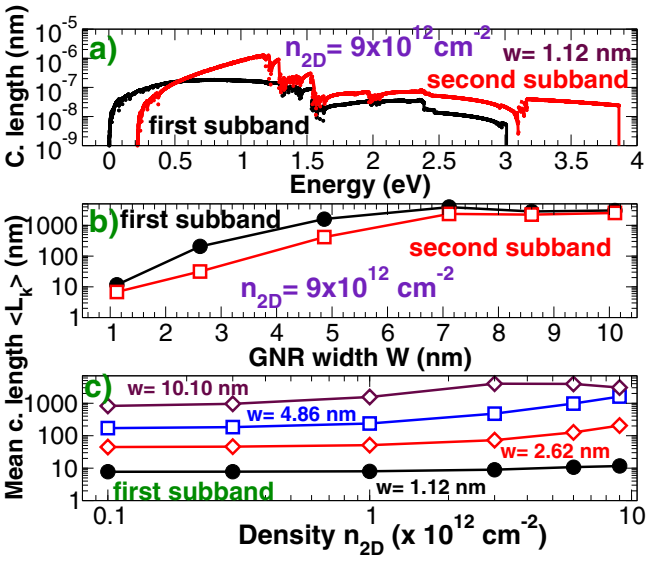

Fig. 9. (a): Coherence length $L_{\mathbf{k}}$ as a function of the electron energy for $W = 1.12$ nm. (b): mean coherence length $\langle L_{\mathbf{k}} \rangle$ as a function of W. In (a) and (b) data for the lowest two conduction subbands are shown and $n_{2D} = 9 \times 10^{12}$ cm^{-2}. (c): $\langle L_{\mathbf{k}} \rangle$ for an electron in the lowest conduction subband as a function of n_{2D} for different W.

IV. Final Remarks

In conclusion, the main learnings are: i) a full band treatment of electrons and phonons is essential to obtain accurate results. On the other hand, forward scattering can be neglected up to widths of 10 nm. ii) Lateral confinement suppresses the intrinsic mobility of GNRs with respect to a graphene sheet. However, phonon-limited mobility of GNRs is 1-2 orders of magnitude higher than that of comparable silicon nanowires. iii) The coherence length of narrow GNRs is as low as 10 nm, therefore the ballistic transport assumption is not fully justified for narrow GNRs. iv) Phonon-limited mobility is at least one order of magnitude higher than mobility observed experimentally in GNRs: new defect-free fabrication methods could close the gap.

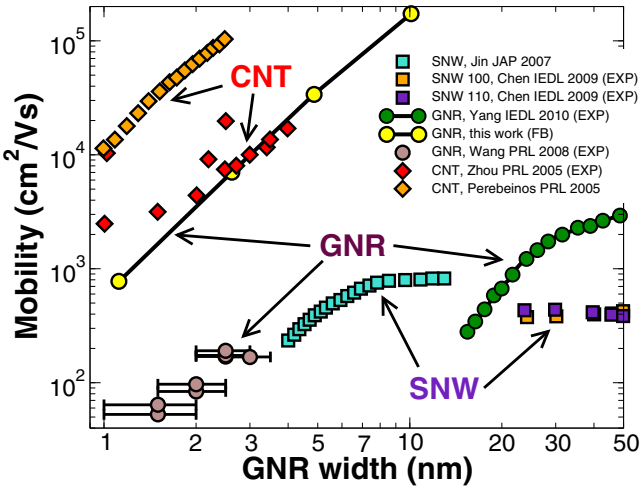

Fig. 10. Mobility as a function of W for different quasi-1D devices: GNR, Carbon NanoTube (CNT) and Silicon NanoWire (SNW). Results from experiments (EXP), simulations and our calculated data for GNR phonon-limited mobility are shown.

V. Acknowledgments

This work was supported in part by the EC 7FP through the Network of Excellence NANOSIL (Contract 216171), by the Project GRAND (Contract 215752), by the European Science Foundation EUROCORES Programme Fundamentals of Nanoelectronics, through funding from the CNR (awarded to IEEIIT-PISA) and the EC 6FP, under Project Dewint (Contract ERASCT- 2003-980409), and by the MIUR-PRIN "Modeling and simulation of graphene nanoribbon FETs for high-performance and low-power logic applications" project (Prot. 2008S2CLJ9).

References

[1] L. Jiao et al., "Facile Synthesis of High Quality Graphene Nanoribbons", http://arxiv.org/abs/1004.1228, *Nature Nanotechnology in press, 2010*.
[2] Y.-W. Son et al., "Energy Gaps in Graphene Nanoribbons", *Phys. Rev. Lett.*, Vol. 97, p. 216803, 2006.
[3] T. Fang et al., "Mobility in semiconducting graphene nanoribbons: Phonon, impurity, and edge roughness scattering", *Phys. Rev. B*, Vol. 78, p. 205403, 2008.
[4] M. Bresciani et al., "Simple end efficient modeling of the E-k relationship and low-field mobility in Graphene Nano-Ribbons", *Solid-State Electronics*, vol. 54, p. 1015, 2010.
[5] A. Betti et al., "Physical insights on graphene nanoribbon mobility through atomistic simulations", *IEDM Tech. Digest*, p. 897-900, 2009.
[6] L. Wirtz et al., "The phonon dispersion of graphite revised", *Solid State Communications*, Vol. 131, p. 141, 2004.
[7] A. V. Rozhkov et al., "Electronic properties of armchair graphene nanoribbons", *Phys. Rev. B* Vol. 79, p. 125420, 2009.
[8] R. Mickevicius et al, "Acoustic-phonon scattering in a rectangular quantum wire", *Phys. Rev. B* Vol. 48, p. 17194, 1993.
[9] R. Kubo, "Statistical-Mechanical Theory of Irreversible Processes", *J. Phys. Soc. Jpn.*, Vol. 12, p. 570, 1958.
[10] E. Mariani et al, "Flexural Phonons in Free-Standing Graphene", *Phys. Rev. Lett.* Vol. 100, p. 076801, 2008.
[11] A. C. Ferrari et al, "Raman Spectrum of Graphene and Graphene Layers", *Phys. Rev. Lett.* Vol. 97, p. 187401, 2006.
[12] K. M. Borysenko et al, "First Principles Analysis of Electron-Phonon Interactions in Graphene", *Phys. Rev. B* Vol. 81, p. 121412, 2010.
[13] J. L. Manes, "Symmetry-based approach to electron-phonon interactions in graphene", *Phys. Rev. B* Vol. 76, p. 045430, 2007.
[14] R. S. Shishir et al, "Intrinsic mobility in graphene", *J. Comput. Electron.* Vol. 8, p. 43, 2009.
[15] K. I. Bolotin et al, "Temperature-Dependent Transport in Suspended Graphene", *Phys. Rev. Lett.* Vol. 101, p. 096802, 2008.
[16] V. Perebeinos et al, "Electron-Phonon Interaction and Transport in Semiconducting Carbon Nanotubes", *Phys. Rev. Lett.* Vol. 94, p. 086802, 2005.